CORRELATION DEVELOPMENT AND PARAMETRIC INVESTIGATION FOR LOCAL PRESSURE DROP OF MIXING T-JUNCTION USING RESPONSE SURFACE METHODOLOGY

Changshuang ZHI[a,*], Erqiang CHEN[a], Shaofeng ZHANG[a], Buting ZHANG[a], Zhenping LI[a], Shun YOU[a], Yingwen LIU[b,*]

[a] State Grid Henan Electric Power Research Institute, Zhengzhou, 450052, Henan, China

[b] School of Energy and Power Engineering, Xi'an Jiaotong University, Xi'an, 710049, China

[*] Corresponding author; E-mail: zhichangshuang2020@163.com, ywliu@xjtu.edu.cn

The behavior of mixing flow within a T-junction is highly intricate in energy transport systems. A 3D numerical model for the T-junction was established, the flow and thermal characteristics were analyzed in detail. The response surface methodology was employed to investigate the interactive effects of angle, velocity ratio, and diameter ratio on the local pressure drop coefficients of the T-junction. The corresponding correlations for K_{AC} and K_{BC} were developed and validated. It could be observed that, compared with the inlet pressures of the main and branch tubes, the static pressure in the downstream section of the main tube drops sharply. A symmetrical vortex can be found at the entrance of the downstream in main tube. Three key parameters including cos θ, U, and D* all have a significant effect on K_{AC} and K_{BC}, and the interactions of cos θ with U* and D* are significant for K_{AC}, while for K_{BC}, the interactions among the three parameters are all significant. Furthermore, the developed correlations demonstrate high accuracy in predicting the local pressure drop coefficients. To validate their reliability, two additional tests are conducted. The discrepancies between the simulated and predicted values of K_{AC} are merely 1.46% and 7.39% for the first and second tests, respectively, while those for K_{BC} are limited to 9.7% and 7.02%, respectively.*

Keywords: *T-junction; Mixing characteristics; Local pressure drop; Response surface methodology; Correlation*

1. Introduction

T-junctions are extensively used in transportation systems, such as nuclear power, chemical and thermal systems [1]. According to different flow configurations, it can be divided into diverging T-junction and mixing T-junction [2]. In this paper, the focus will be on the mixing behaviors in T-junction. When two fluid streams with different temperatures mix in T-junction, particular attention should be given to two key aspects: thermal characteristics and flow pressure drop [3]. The following summarizes the research progress in these two aspects.

The research of mixing characteristic in T-junction originated from thermal fatigue in the nuclear power. Temperature fluctuation-induced thermal fatigue is a major contributor to material degradation in nuclear power plants, posing a significant risk of loss-of-coolant accidents. To prevent and mitigate temperature fluctuations in T-junction, numerous researchers have conducted extensive studies to

evaluate the mechanisms and characteristics of thermal mixing. Kamide et al. [4] performed a water experiment to investigate thermal striping phenomena. The jet flow patterns are categorized into three distinct forms: wall jet, deflecting jet, and impinging jet. Notably, in cases involving an impinging jet, a cold spot developed on the upper surface downstream of the main pipe, whereas for the wall jet, a similar phenomenon occurred on the lower surface. Furthermore, they also analyzed the velocity and temperature field distributions of three flow patterns and highlighted that the flow regime is determined by the momentum ratio between the branch tube and the main tube. Lee et al. [5] summarized that the temperature difference and the increase in heat transfer coefficient caused by turbulent mixing are the key factors leading to thermal fatigue failure. However, Wang et al. [6] believed that the effect of temperature difference on temperature fluctuations is limited for the T-junction with porous media. Lu and his team have done a lot of work on the T-junction, including the mathematical simulation methods, the installation of distributors and porous, the definition of the mean and root temperature and velocity, and laying the groundwork for subsequent studies on thermal mixing prediction [7-11]. In short, the researches on thermal mixing are extensive and well developed.

Currently, most studies on pressure drop in T-junctions are based on experimental results. Abou-Haidar et al. [12] pioneered the study of mixed flow in T-junctions and conducted a visualization study using dry air as the working fluid. It can be revealed that the maximum Mach number after flow merging could reach 0.66. Bassett et al. [13] developed expressions to calculate steady flow pressure loss coefficients for mixing and dividing flow in T-junction through experiments. Schmandt et al. [14] and Herwig et al. [15] determined the pressure loss coefficients for mixing laminar flow in square cross-section T-junctions based on a Second Law analysis, and highlighted the limitations of the previous model due to its underlying assumptions. Furthermore, Pérez-García et al. [16] conducted experimental and numerical studies on compressible flow in 90° T-junction, incorporating Mach number as an additional independent parameter in the correlation. In addition to experiments, numerical simulation is also a commonly method. For instance, Gan and Riffat. [17] conducted numerical simulations to investigate the pressure loss characteristics of air flow in square-section T-junction, and concluded that the pressure loss coefficient is a function of the flow rate ratio, with the branch exhibiting a negative loss coefficient at low flow rate ratios. Abdulwahhab et al. [18] studied the pressure loss in a 90° T-junction and found that as the flow ratio increases, the pressure loss in the main tube significantly increases, and illustrated the interaction between flow ratio and area ratio. Patiño-Jaramillo et al. [19] investigated the flow characteristics and pressure loss of a 90° T-junction under laminar flow, and revealed the coexistence of three recirculation zones (A/C/D) in mixing flow, with a particular focus on its application in the cooling oil flow of oil-immersed power transformer windings.

Despite extensive researches on mixing T-junctions, most studies have focused on thermal performance, with relatively few addressing pressure drop. Some researchers have pointed out that the interaction between parameters has a significant effect on the local resistance coefficient. However, studies on these interactions remain scarce. The author had previously studied the resistance characteristics in a diverging T-junction, analyzed the local pressure drop for liquid-liquid two-phase flow [20] and gas-liquid two-phase flow [21], and obtained correlation equations. This will lay the foundation for the analysis of mixing T-junction in this study. Therefore, this study aims to explore the interaction effects of three key parameters, including velocity ratio, diameter ratio, and angle on the local resistance coefficients, by introducing a response surface methodology and a nonlinear regression model with quadratic terms. The correlations would be proposed to provide a reference for the optimal design of pipeline systems.

2. Methodology

2.1. Physical model

Figure 1 illustrates a schematic representation of the mixing T-junction, consisting of a main tube and a branch tube. The main tube is aligned horizontally, while the branch tube extends upward, intersecting at a certain angle at the origin. The main tube includes the upstream of the inlet section and the downstream of the outlet section, with lengths of 10 and 20 times the tube diameter, respectively. The branch tube is also an inlet section, with a length of 10 times the diameter of the tube. The working fluid utilized in this study is water, with a temperature of 321.15K at the inlet of the main tube and 306.15K at the inlet of the branch tube. The gravity vertically downwards along the *x*-axis. The fluid in the main and branch tubes converges at the intersection of the T-junction, and fluctuations in flow and thermal performance occur at the intersection of the T-junction. In order to better analyze the flow and thermal performance, a line in the symmetrical plane (*x*-*y* plane) is defined at distance of 0.5*D*, and its velocity, pressure, temperature, and other characteristics along the line could be characterized.

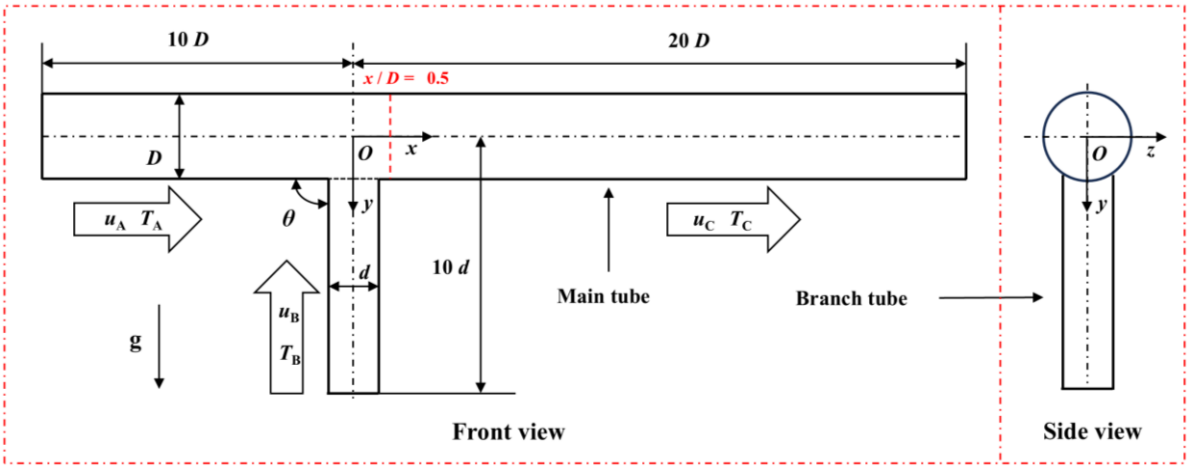

Figure 1. Schematic representation of the mixing T-junction

2.2. Mathematical method

Under the present study, the numerical simulation of the T-junction was conducted using a steady-state approach. The inlet and outlet of the T-junction were respectively the velocity inlet and pressure outlet. The wall adopted a non-slip and non-equilibrium wall. The wall was set to be adiabatic. Considering the relatively small variations in density, buoyancy effects were modeled using the boussinesq approximation, and the operating density was set to 994.9 kg·m^{-3}. The governing equations, comprising the continuity, energy, and momentum, could be formulated as follows:

$$\frac{\partial\left(\rho u_i\right)}{\partial x_i}=0 \tag{1}$$

$$\frac{\partial\left(\rho u_i T\right)}{\partial x_i}=\frac{\partial}{\partial x_i}\left(\left(\frac{\mu_t}{Pr_T}+\frac{\mu}{Pr}\right)\frac{\partial T}{\partial x_i}\right) \tag{2}$$

$$\frac{\partial\left(\rho u_i u_j\right)}{\partial x_j}=\frac{\partial}{\partial x_j}\left(\left(\mu+\mu_t\right)\left(\frac{\partial u_i}{\partial x_j}+\frac{\partial u_j}{\partial x_i}\right)\right)-\frac{\partial p}{\partial x_i}-\frac{2}{3}\delta_{ij}\left(\mu+\mu_t\right)\frac{\partial u_k}{\partial x_k}+\rho g_i \tag{3}$$

where μ_t is turbulent viscosity respectively, which can be calculated as follows:

$$\mu_t = \rho C_\mu \frac{k^2}{\varepsilon} \tag{4}$$

The turbulence model is the standard k-ε model, and its formulation is provided as follows:

$$\frac{\partial(\rho u_i k)}{\partial x_i} = \frac{\partial}{\partial x_i}\left[(\mu + \mu_t)\frac{\partial k}{\partial x_i}\right] + G_k - \varepsilon \tag{5}$$

$$\frac{\partial(\rho u_i \varepsilon)}{\partial x_i} = \frac{\partial}{\partial x_i}\left[(\mu + \mu_t)\frac{\partial \varepsilon}{\partial x_i}\right] + C_1 \frac{\varepsilon}{k} G_k - C_2 \rho \frac{\varepsilon^2}{k} \tag{6}$$

$$G_k = \mu_t \frac{\partial u_i}{\partial x_j}\left(\frac{\partial u_i}{\partial x_j} + \frac{\partial u_j}{\partial x_i}\right) \tag{7}$$

where C_1 controls the balance between the generation and dissipation of turbulent kinetic energy, while C_2 governs the rate of energy dissipation. These constants are empirically derived and have been validated for a range of fluid dynamics applications. The C_1 and C_2 are constants with values of 1.44 and 1.92, respectively. They were selected based on the standard values used in the standard k-ε model, which had been confirmed by combining the experimental data in previous research in T-junction [22].

2.3. Meshing and model validation

The numerical simulations of the T-junction were performed using the finite volume method. The governing equations for fluid flow and heat transfer were solved with the SIMPLE algorithm for pressure-velocity coupling, and the spatial discretization was carried out using the least squares cell based method. For the discretization of the momentum and energy equations, the second order upwind scheme was selected, ensuring both stability and accuracy of the solution. It is necessary to conduct a grid independence study to verify the accuracy and reliability of the results. Compared with tetrahedral grids, hexahedral grids offer high computational efficiency, better accuracy, and easier data storage due to their regular structure. The grid division with hexahedral grids in the intersection of T-junction was generated, as shown in Fig. 2. Three different grid schemes were divided for the T-junction, including 1.06 million, 2.14million and 2.98 million, as shown in Fig. 2. The velocity distributions along the line of $x/D = 0.5$ under different grid numbers were compared. It can be observed that the minimum velocity occurs at x = -0.05 m. As the grid number increases from 1.06 million to 2.14 million, the change of the minimum velocity is relatively more noticeable (-0.178 m·s^{-1} to -0.212 m·s^{-1}), but as the grid number increases further from 2.14 million to 2.98 million, the velocity distribution undergoes minimal changes (-0.212 m·s^{-1} to -0.22 m·s^{-1}), indicating that the solution has largely converged with the finer grid. Since the comparison is conducted in a region with high turbulence intensity, the grid with 2.14 million cells is selected as the final grid scheme.

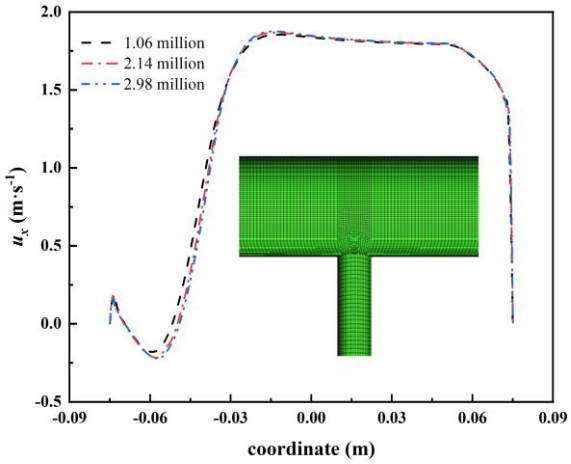

Figure 2. Meshing and grid independence verification

Figure 3 presents a comparative analysis between simulation results and benchmark experimental data from Kamide et al. [4] along the line of x/D = 0.5, with particular focus on thermal and flow characteristics as manifested through temperature profiles and velocity distributions. The conditions of experiment and simulation are consistent. The inlet velocity of main tube was assigned as 1.46 m·s^{-1}, and that of branch tube was assigned as 1.0 m·s^{-1}. The temperatures of the main and branch tube were assigned as 321.15 K and 306.16 K, respectively. It is evident that the temperature and velocity distributions are in good qualitative and quantitative agreement with that in the experiment.

Minor discrepancies of the temperature and velocity occur in the range of y = -0.075 m ~ -0.03 m. In the current range, the simulated temperature is lower than the experimental value, and the simulated velocity is greater than the experimental value, which might be attributed to the velocity with 5% turbulence intensity was performed to the inlet, while there was about 10% fluctuation intensity of the average velocity in the experiment [23]. In short, this area happens to be on the right side of the intersection between the branch tube and the main tube, where vortices will form during mixing, resulting in significant fluctuations in physical variables and corresponding errors in experimental measurements. Overall, the simulation results in this study are highly consistent with the experiment. Consequently, the employed numerical model was retained for the computation of subsequent scenarios.

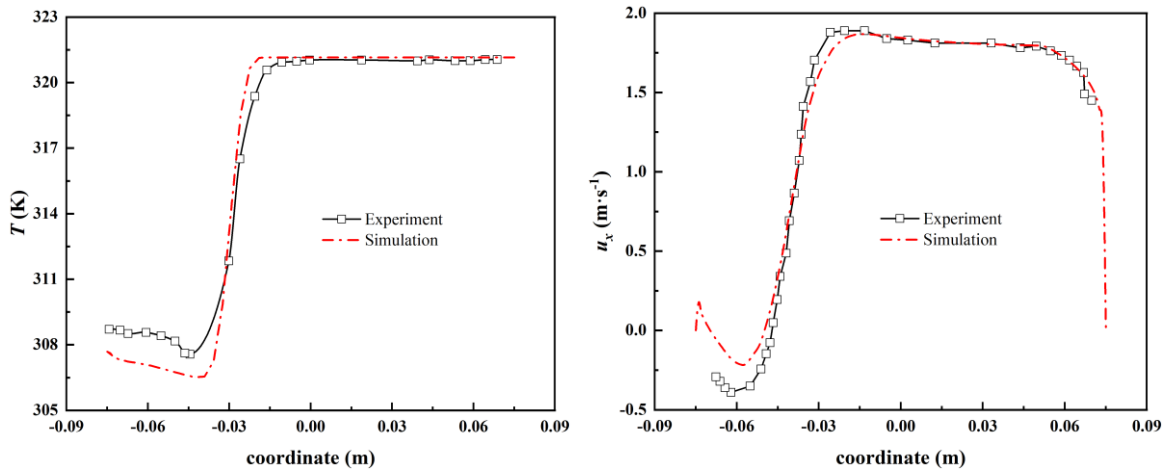

(a) Temperature distribution *(b) Velocity distribution*

Figure 3. Comparison between simulation results and experimental values

2.4. Parameter definition

Figure 4 illustrates the static pressure distribution along the T-junction. Upon entering the main or branch tube, the fluid's pressure gradually decreases due to friction. At the intersection, the pressure experiences a sharp drop, followed by a brief increase, before transitioning into the fully developed region. The static pressure difference observed at the junction arises from both reversible and irreversible pressure drops.

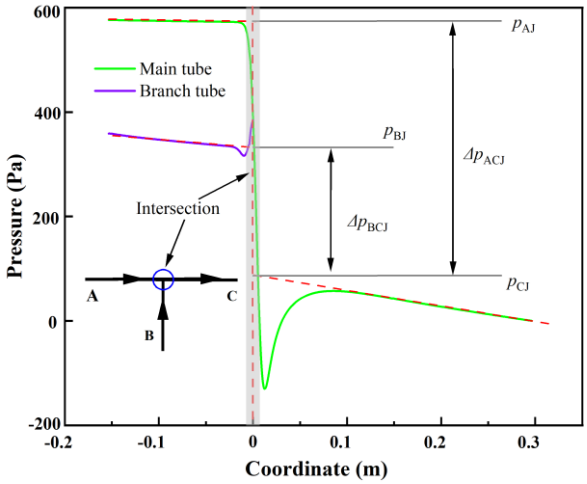

Figure 4. Pressure distribution along the T-junction

Δp_{ACJ} represents the local pressure at the intersection between the upstream and downstream of the main tube. Δp_{BCJ} represents the local pressure at the intersection of branch tube and the downstream. Therein, p_{AJ}, p_{BJ}, and p_{CJ} are the pressure values at the intersection of the centerline where the pressure distribution in the corresponding pipes is linearized and intersects [24, 25]. After obtaining the local pressure drop through numerical simulations, the local pressure drop coefficients including K_{AC} and K_{BC}, can be solved as follows:

$$\Delta p_{ACJ} = p_{AJ} - p_{CJ} = \frac{G_A^2}{2\rho} - \frac{G_C^2}{2\rho} + K_{AC} \cdot \frac{G_C^2}{2\rho} \tag{8}$$

$$\Delta p_{BCJ} = p_{BJ} - p_{CJ} = \frac{G_B^2}{2\rho} - \frac{G_C^2}{2\rho} + K_{BC} \cdot \frac{G_C^2}{2\rho} \tag{9}$$

2.5. Response surface methodology

Response Surface Methodology (RSM) is an integrated analytical approach that merges statistical techniques with mathematical modeling. Table 1 shows the test matrix design, which includes 24 sets of data. Three dimensionless factors (velocity ratio U^*, diameter ratio D^*, cos θ) are selected as independent variables, and two local pressure drop coefficients K_{AC} and K_{BC} are used as output variables. The velocity ratio U^* and diameter ratio D^* can be calculated as follows:

$$U^* = \frac{u_A}{u_B} \tag{10}$$

$$D^* = \frac{d}{D} \tag{11}$$

In this study, there is a strong non-linear characteristic between the independent variable and the output variable, so it is necessary to introduce the regression model with interaction term and quadratic term based on the linear model. A modified two-factor interaction model and the modified quadratic regression model are shown follows [26]:

$$y = \beta_0 + \sum_{i=1}^{k} \beta_i x_i + \sum_{i=1}^{k-1} \sum_{j=2}^{k} \beta_{ij} x_i x_j + \varepsilon \tag{12}$$

$$y = \beta_0 + \sum_{i=1}^{k} \beta_i x_i + \sum_{i=1}^{k-1} \sum_{j=2}^{k} \beta_{ij} x_i x_j + \sum_{i=1}^{k} \beta_{ii} x_i^2 + \varepsilon \tag{13}$$

where β_0, β_i, βij and β_{ii} refer to coefficients for the intercept, linear, interaction and quadratic terms respectively, and ε is a total error including random error, modeling error and systematic error. In this study, the modified two-factor interaction model and modified quadratic regression model were used to develop the correlations for K_{AC} and K_{BC}, respectively.

Table 1. The design of test matrix for RSM

Cases	cos θ	U^*	D^*	Cases	cos θ	U^*	D^*
1	0.7071	1	1	13	0.7071	1	0.6667
2	-0.7071	1	1	14	0.7071	0.5	1
3	0	1	0.6667	15	0.7071	1.5	1
4	0	1.5	1	16	0	1	0.3333
5	-0.7071	1.5	0.6667	17	0	0.5	0.6667
6	0	0.5	1	18	0	1	0.6667
7	0.7071	0.5	0.6667	19	0	1	1
8	0	1.5	0.3333	20	-0.7071	0.5	0.3333
9	0.7071	1.5	0.6667	21	-0.7071	1.5	0.3333
10	0.7071	1	0.3333	22	-0.7071	1	0.6667
11	-0.7071	1	0.3333	23	-0.7071	0.5	1
12	0.7071	1.5	0.3333	24	-0.7071	1.5	1

3. Results and discussion

3.1. Analysis of flow and thermal characteristics

Figure 5 illustrates the temperature distribution at the intersection of the T-junction. It is evident that as the angle between the branch tube and the upstream of the main tube increases, the temperature mixing uniformity in the downstream of main tube improves. At small angles, the velocity vectors of the main tube and branch tube at the inlet are aligned in the horizontal direction, resulting in cooperative velocities that hinder efficient mixing and cause noticeable temperature stratification. Conversely, at larger angles, the velocity components of the two inlets oppose each other in the horizontal direction. It leads to more effective mixing of the fluid streams downstream of the main tube, thereby enhancing temperature uniformity. Additionally, for a given angle, an increase in the diameter ratio further improves the temperature mixing uniformity in the downstream of the main tube. It is primarily due to the increased flow rate of the branch tube as its diameter increases, which intensifies turbulence of the main tube, which promotes the uniformity of temperature mixing.

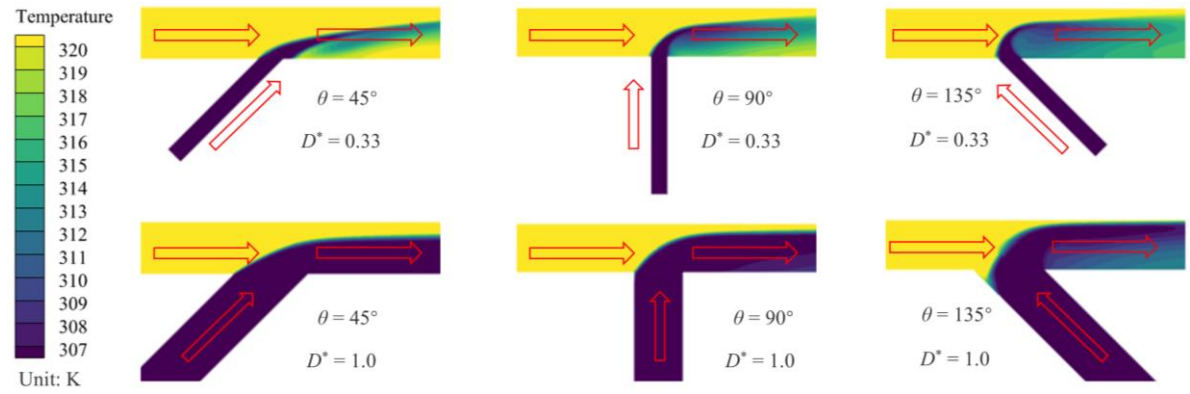

Figure 5. Temperature distribution at the intersection of T-junction

Figure 6 presents the pressure distribution and streamline patterns at both $z = 0$ and $y = -0.045$ m within the intersection region. It can be observed that compared with the inlet pressures of the main tube and branch pipe, the static pressure in the downstream of the main tube undergoes a rapid decrease. This phenomenon can be explained through the following mechanisms. Firstly, when the fluids from the main tube and branch tube pass through the T-junction, the flow rate and velocity in the downstream of the main tube increase significantly, resulting in the conversion of static pressure to dynamic pressure and consequent reduction in static pressure. Secondly, at smaller intersection angles, the streamlines in the T-junction exhibit relatively smooth trajectories. With increasing intersection angle, the fluids from the main tube and branch tube develop opposing tangential force components. The accelerated flow near the upper wall of the main tube generates centrifugal motion relative to the vortical fluid, leading to the formation of a vortex near the lower wall at the downstream entrance of the main tube, as indicated by the vortex highlighted in the red circle. This vortex formation contributes to localized pressure reduction. Additionally, the vortex at the $y = -0.045$ m demonstrates pronounced symmetry characteristics.

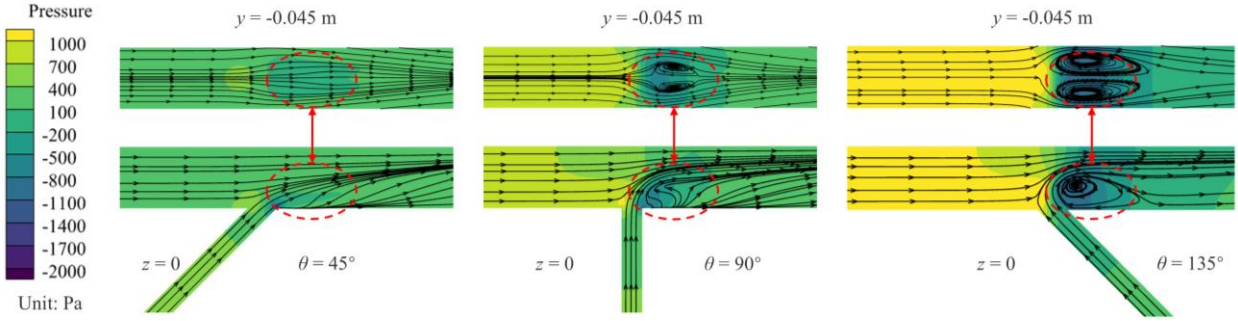

Figure 6. Pressure and streamline distributions at different angles

3.2. Analysis of variance (ANOVA)

Analysis of variance (ANOVA) was employed to examine the statistical significance of three key parameters on the local resistance coefficient. Tables 2 and 3 present the ANOVA results for K_{AC} and K_{BC}, respectively. The Adj R^2 and Pred R^2 for K_{AC} are 0.9761 and 0.9613, respectively, while those for K_{BC} are 0.9473 and 0.9154. Since the differences between Adj R^2 and Pred R^2 are all far below 0.2, the regression models effectively reveal the effects of independent variables on the dependent variable [27]. Furthermore, "Adeq Precision" measures the signal to noise ratio. The ratios for K_{AC} and K_{BC} are 43.86 and 24.73, respectively, both well above the threshold of 4, further reinforcing the reliability of the model [28].

During the regression model fitting process, a 95% confidence interval is applied. Consequently, a p-Value below 0.05 signifies statistical significance and is denoted by a "Y". It can be seen that for K_{AC}, the three key parameters including cos θ, U^*, and D^* all have a significant effect on K_{AC}, and the interactions of cos θ with U^* and D^* are both significant. For K_{BC}, the interactions among the three parameters are all significant.

Table 2. ANOVA of K_{AC}

Source	Sum of squares	*df*	Mean Square	F Value	p-Value	Significance
Model	2.44	6	0.4074	157.5	< 0.0001	Y
A - cos θ	1.66	1	1.66	640.88	< 0.0001	Y
B - U^*	0.032	1	0.032	12.36	0.0027	Y
C - D^*	0.3438	1	0.3438	132.91	< 0.0001	Y
AB	0.2114	1	0.2114	81.7	< 0.0001	Y
AC	0.1453	1	0.1453	56.16	< 0.0001	Y
BC	0.011	1	0.011	4.25	0.0549	N
Residual	0.044	17	0.0026			
Cor Total	2.49	23				
Adj R^2=0.9761			Adeq Precision = 43.86			
Pred R^2=0.9613						

Table 3. ANOVA of K_{BC}

Source	Sum of squares	*df*	Mean Square	F Value	p-Value	Significance
Model	3.9	9	0.4335	46.89	< 0.0001	Y
A - cos θ	0.8038	1	0.8038	86.95	< 0.0001	Y
B - U^*	2	1	2	216.32	< 0.0001	Y
C - D^*	0.1442	1	0.1442	15.6	0.0015	Y
AB	0.0466	1	0.0466	5.04	0.0414	Y
AC	0.2616	1	0.2616	28.29	0.0001	Y
BC	0.3144	1	0.3144	34.01	< 0.0001	Y
A^2	0.0025	1	0.0025	0.2657	0.6143	N
B^2	0.1362	1	0.1362	14.74	0.0018	Y
C^2	0.0064	1	0.0064	0.6885	0.4206	N
Residual	0.1294	14	0.0092			
Cor Total	4.03	23				
Adj R^2=0.9473			Adeq Precision = 24.37			
Pred R^2=0.9154						

3.3. Interactive effects of parameters

Figure 7 (a) illustrates the interaction between cos θ and U^* on K_{AC}. It can be observed that as the cos θ decreases, i.e., as the angle increases, the local pressure drop coefficient K_{AC} gradually increases, it can be explained as follows. With the increase in angle, the relationship between the velocity in the branch tube and the velocity in the main tube shifts from synergy to impact, leading to a gradual increase

in energy loss at the intersection of the T-junction. Additionally, when the angle is small, K_{AC} slightly increases with the increase in the U^*. However, when the angle is large, K_{AC} decreases with the increase in the U^*.

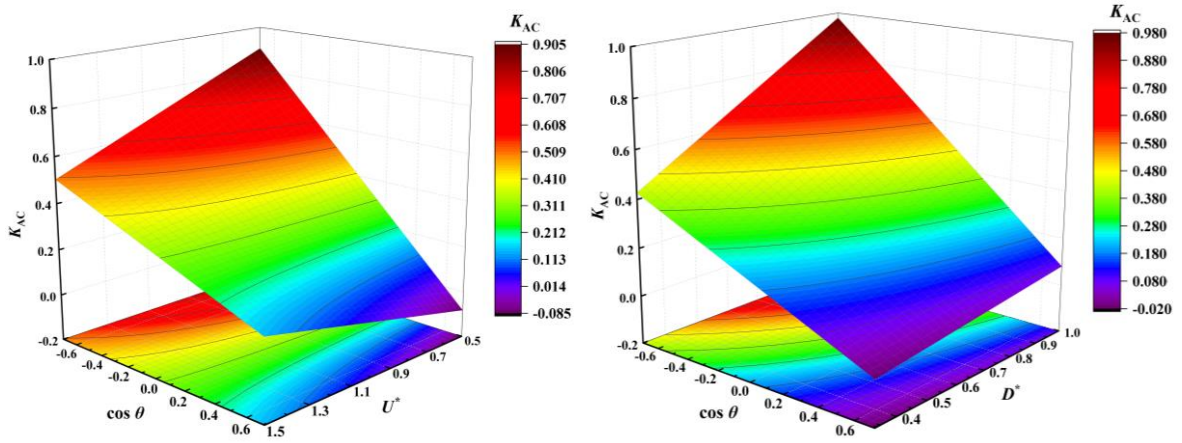

(a) Interactive effect of cos θ and U^* *(b) Interactive effect of cos θ and D^**

Figure 7. The response surface 3D plot of K_{AC}

Figure 7 (b) presents the interaction between cos θ and D^*, showing that K_{AC} gradually increases with the increase in the D^*. As the diameter ratio increases, the flow rate in the branch tube also increases, resulting in higher turbulence intensity at the T-junction intersection. Moreover, when the angle is small, the effect of the diameter ratio on the local pressure drop coefficient is minimal, whereas when the angle is large, the influence of the diameter ratio on K_{AC} becomes more pronounced.

Figure 8 (a) demonstrates the interaction between cos θ and U^* on K_{BC}. It can be seen that as cos θ decreases, i.e., as the angle increases, K_{BC} gradually increases. Moreover, when the velocity ratio is relatively low, the effect of angle is more pronounced. Additionally, it can be seen that as the velocity ratio increases, the K_{BC} gradually decreases. It can be explained as follows. With the velocity ratio increases, the turbulence intensity at the intersection of the T-junction rises, leading to an increase in local pressure loss. However, at the same time, the downstream flow rate and the total dynamic pressure in the main tube also increase, playing a dominant role, which ultimately results in a reduction of the local resistance coefficient K_{BC}. Figure 8 (b) illustrates the interactive effect of cos θ and D^* on K_{BC}. When the angle is relatively small, K_{BC} decreases slightly with an increasing diameter ratio. In this case, the increase in the downstream dynamic pressure of the main tube becomes dominant, leading to a reduction in the local pressure loss coefficient. However, when the angle is large, the turbulence intensity at the intersection of the T-junction increases with the diameter ratio and becomes the dominant factor, resulting in a gradual increase in K_{BC} as the diameter ratio increases.

According to Fig. 8 (c), it can be found that the U^* has a strong interaction with the D^* in influencing the K_{BC}. When the diameter ratio is small, the velocity ratio has a more significant effect on the K_{BC}, whereas when the diameter ratio is large, the influence of the velocity ratio becomes less pronounced. Additionally, when the velocity ratio is relatively low, K_{BC} decreases slightly with an increasing diameter ratio. Under low velocity ratio conditions, the flow velocity in the main tube is relatively low, and an increase in the diameter ratio leads to a more noticeable increase in main pipe velocity, thereby reducing K_{BC}. However, when the velocity ratio is high, the flow rate in the main tube is already at a relatively high level. In this case, the effect of the diameter ratio on increasing the main tube velocity becomes less significant, while the intensification of turbulence at the intersection of the T-junction becomes the dominant factor, leading to an increase in the K_{BC}.

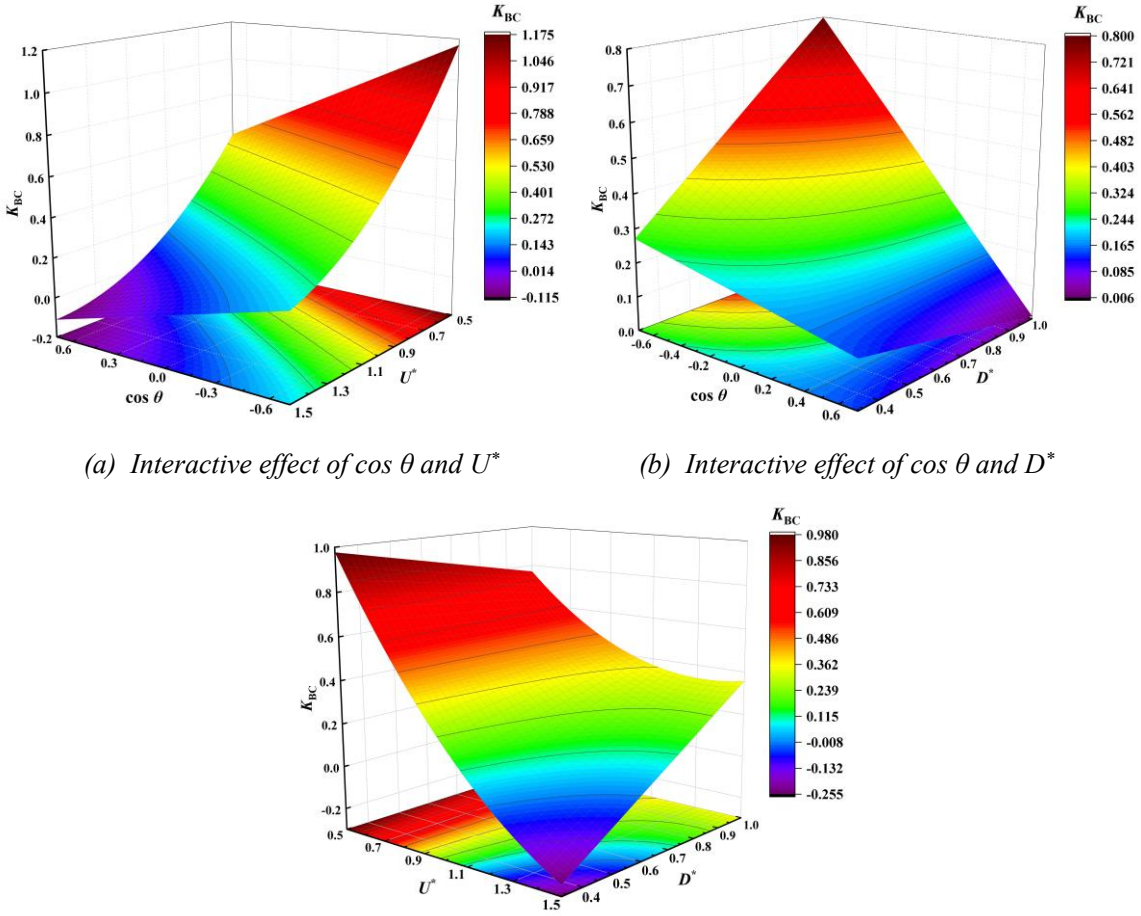

(a) Interactive effect of cos θ and U^* *(b) Interactive effect of cos θ and D^**

(c) Interactive effect of U^* and D^*

Figure 8. The response surface 3D plot of K_{BC}

3.4. Regression models of responses

Using the RSM and ANOVA, the regression models with the interactions have been developed. During the model construction process, only the terms with significant contributions are retained to ensure the model's conciseness and accuracy. As a result, the correlations for K_{AC} and K_{BC}, considering three dimensionless factors, are derived as follows:

$$K_{AC} = 0.13 + \left(0.44U^* - 0.6\right)\cos\theta - 0.09U^* + \left(0.49 - 0.48\cos\theta\right)D^* \quad (14)$$

$$K_{BC} = 2.38 + \left(0.19U^* - 0.05\right)\cos\theta + \left(1.22D^* + 0.64U^* - 2.91\right)U^* - \left(0.93 + 0.7\cos\theta\right)D^* \quad (15)$$

Figure 9 presents a comparison between the predicted values from the RSM regression model and the simulated results. It can be observed that the data points are uniformly distributed around the diagonal for K_{AC} and K_{BC}, indicating that the errors between the simulated and predicted data are minimal. Since the local resistance values remain at a relatively low level, standardized residuals are utilized to assess the magnitude of prediction errors [29], as shown in Fig. 10. For K_{AC} and K_{BC}, the thresholds of their standardized residuals are ±3.627 and ±3.713, respectively. The standardized residuals of both K_{AC} and K_{BC} do not exceed their corresponding thresholds, indicating that the correlations obtained from the response surface methodology can accurately predict the local resistance

coefficients of the T-junction.

Two additional tests were conducted to further validate the accuracy of the correlations obtained through the RSM, and these two tests were not included in the original design matrix. The local resistance coefficients obtained from the correlations were compared with those derived from simulations, as presented in Tab. 4. It can be observed that the errors between the simulation and predicted values of K_{AC} for the first and second tests are only 1.46% and 7.39%, respectively, and the errors for K_{BC} are only 9.7% and 7.02%, respectively. It indicates that the correlations exhibit good predictive capability within the given parameter range.

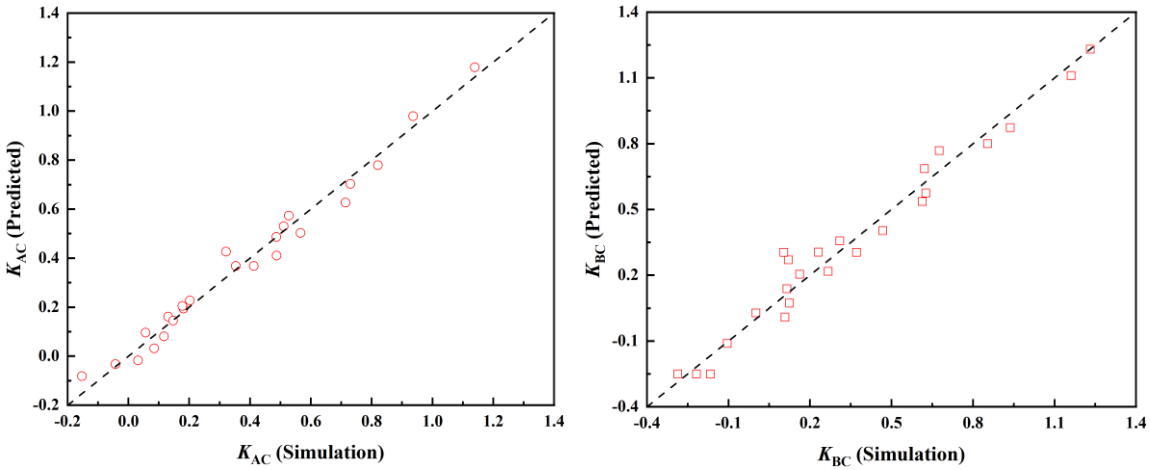

(a) K_{AC} *(b)* K_{BC}

Figure 9. Comparison of predicted and simulation data

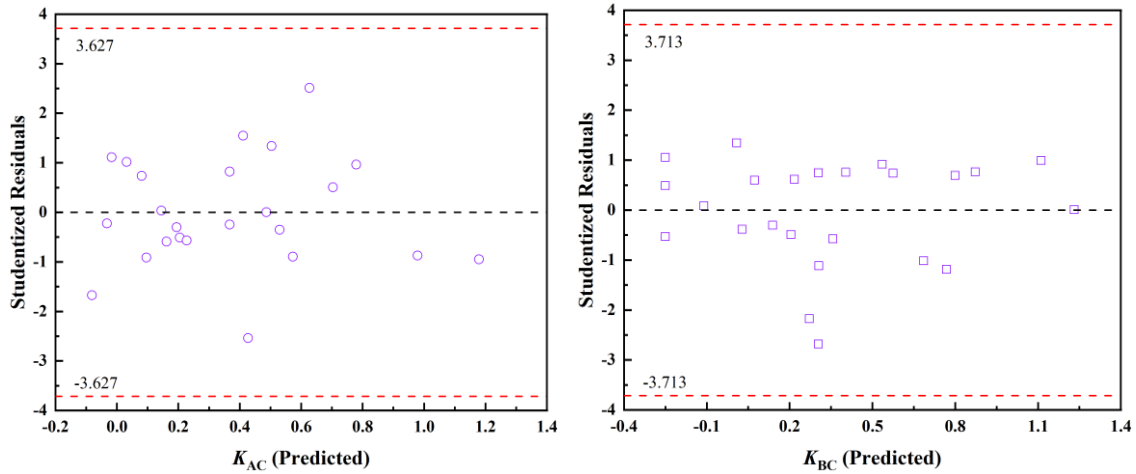

(a) K_{AC} (b) K_{BC}

Figure 10. Comparison of predicted and simulation data

Table 4. Additional testing verification results

Cases	cos θ	U^*	D^*	K_{AC} (Simulation)	K_{AC} (Predicted)	Error	K_{BC} (Simulation)	K_{BC} (Predicted)	Error
1	0.5	0.75	1.00	0.181	0.179	1.46%	0.269	0.243	9.70%
2	-0.5	0.55	0.33	0.540	0.500	7.39%	1.049	0.975	7.02%

4. Conclusions

The flow and thermal characteristics of mixing flow in a T-junction were analyzed using numerical simulation, and RSM was employed to investigate the interactive effects of angle, velocity ratio, and diameter ratio on the local pressure drop coefficients of the T-junction. The corresponding correlations for K_{AC} and K_{BC} were derived and validated. The correlations developed in this study could serve as a reference for optimizing T-junction design in pipeline systems, helping to reduce pressure drops and improve the overall efficiency of fluid transport systems. The conclusions can be summarized as follows:

1) The distributions of temperature and pressure were described in detail. As the angle and diameter ratio increase, temperature fluctuations in the downstream region decrease. Compared with the inlet pressures of the main and branch tubes, the static pressure of the downstream in main tube decreases rapidly. A vortex forms at the entrance of the downstream in main tube, exhibiting a distinct symmetrical characteristic.

2) The interaction terms for the local pressure drop coefficients were obtained using RSM and ANOVA. The signal to noise ratios for K_{AC} and K_{BC} are 43.86 and 24.73, respectively, both well above the threshold of 4. For K_{AC}, the three key parameters including cos θ, U^*, and D^* all have a significant effect, and the interactions of cos θ with U^* and D^* are both significant. For K_{BC}, the interactions among the three parameters are all significant.

3) The correlations incorporating interaction terms were developed for K_{AC} and K_{BC}. The correlations can effectively predict the local pressure drop coefficients of the T-junction. Additionally, two extra sets of tests are conducted to validate the accuracy of the correlations. The errors between the simulation and predicted values of K_{AC} for the first and second tests are only 1.46% and 7.39%, respectively, and the errors for K_{BC} are only 9.7% and 7.02%, respectively.

Nomenclature		**Greek symbols**	
T	temperature, K	θ	angle, ℃
D, d	diameter, m	μ_t	turbulent viscosity, Pa·s
u	velocity, m·s^{-1}	μ	dynamic viscosity, Pa·s
U^*	velocity ratio	ρ	density, kg·m^{-3}
D^*	diameter ratio	Δp_{ACJ}, Δp_{BCJ}	local pressure drop, Pa
p	pressure, Pa	**Subscripts**	
Pr	prandtl number		
Pr_T	turbulent Prandtl number	x, y, z	cartesian coordinates
K_{AC}, K_{BC}	local pressure drop coefficient	A	upstream of main tube
RSM	Response Surface Methodology	B	branch tube
ANOVA	Analysis of Variance	C	downstream of main tube

Acknowledgements

This work was supported by National Key Research and Development Program of China (Grant No. 2022YFE210200) and Science Technology Project of State Grid.

References

[1] Lin, C.H., *et al.*, Investigating thermal mixing and reverse flow characteristics in a T-junction by way of experiments, *Applied Thermal Engineering*, *99* (2016), pp. 1171-1182

[2] Yang, B., *et al.*, State-of-art of branching T-junction: Experiments, modeling, developing prospects and applications, *Experimental Thermal and Fluid Science*, *109* (2019), p. 109895

[3] Lu, T., *et al.*, Large-eddy simulations of velocity and temperature fluctuations in hot and cold fluids mixing in a tee junction with an upstream straight or elbow main pipe, *Nuclear Engineering and Design*, *263* (2013), pp. 32-41

[4] Kamide, H., *et al.*, Study on mixing behavior in a tee piping and numerical analyses for evaluation of thermal striping, *Nuclear Engineering and Design*, *239* (2009), 1, pp. 58-67

[5] Lee, J.I., *et al.*, Numerical analysis of thermal striping induced high cycle thermal fatigue in a mixing tee, *Nuclear Engineering and Design*, *239* (2009), 5, pp. 833-839

[6] Wang, Y., *et al.*, Experimental investigation of the thermal fluctuations in hot and cold fluids mixing in a T-junction filled with spherical particles, *Applied Thermal Engineering*, *71* (2014), 1, pp. 310-316

[7] Gao, K., *et al.*, Experimental investigation and numerical simulation for weakening the thermal fluctuations in a T-junction, *Annals of Nuclear Energy*, *78* (2015), pp. 180-187

[8] Wang, Y., Lu, T., Influence of the particle diameter and porosity of packed porous media on the mixing of hot and cold fluids in a T-junction, *International Journal of Heat and Mass Transfer*, *84* (2015), pp. 680-690

[9] Guo, Z., *et al.*, Monitoring of wall temperature fluctuations for thermal fatigue in a horizontal mixing T-junction pipe, *Progress in Nuclear Energy*, *104* (2018), pp. 298-305

[10] Wang, J., *et al.*, Temperature and pressure oscillations induced by steam direct contact condensation in a T-junction with porous inner-structures, *International Journal of Heat and Mass Transfer*, *168* (2021), p. 120863

[11] Lu, T., *et al.*, Numerical Simulation of Flow and Heat Transfer with Large-Eddy Simulation in a Mixing T-Junction, *Applied Mechanics and Materials*, *152* (2012), pp. 1319-1324

[12] Abou-Haidar, N.I.,S.L. Dixon, Pressure Losses in Combining Subsonic Flows Through Branched Ducts, *Journal of Turbomachinery*, *114* (1992), 1, pp. 264-270

[13] Bassett, M., *et al.*, Calculation of steady flow pressure loss coefficients for pipe junctions, *Proceedings of the institution of mechanical engineers, part C: Journal of Mechanical Engineering Science*, *215* (2001), 8, pp. 861-881

[14] Schmandt, B., *et al.*, Determination of head change coefficients for dividing and combining junctions: A method based on the second law of thermodynamics, *Chemical Engineering Science*, *111* (2014), pp. 191-202

[15] Herwig, H., Schmandt, B., How to Determine Losses in a Flow Field: A Paradigm Shift towards the Second Law Analysis, *Entropy*, *16* (2014), 6, pp. 2959-2989

[16] Pérez-García, J., *et al.*, New coefficient to characterize energy losses in compressible flow at T-junctions, *Applied Mathematical Modelling*, *34* (2010), 12, pp. 4289-4305

[17] Gan, G., Riffat, S.B., Numerical determination of energy losses at duct junctions, *Applied Energy*, *67* (2000), 3, pp. 331-340

[18] Abdulwahhab, M., *et al.*, Numerical prediction of pressure loss of fluid in a T-junction, *International journal of energy and environment*, *4* (2013), 2, pp. 253-264

[19] Patiño-Jaramillo, G.A., *et al.*, Laminar flow and pressure loss in planar Tee joints: Numerical simulations and flow analysis, *European Journal of Mechanics-B/Fluids*, *92* (2022), pp. 75-89

[20] Zhi, C., *et al.*, Numerical investigation of liquid-liquid two-phase separation and pressure drop characteristics

in T-junctions, *The Canadian Journal of Chemical Engineering*, *100* (2022), 2, pp. 363-374
[21] Zhi, C., *et al.*, Numerical analysis and artificial neural network-based prediction of two-phase flow pressure drop of refrigerants in T-junction, *International Journal of Refrigeration*, *137* (2022), pp. 34-42
[22] Wang, S.J., Mujumdar, A.S., Flow and mixing characteristics of multiple and multi-set opposing jets, *Chemical Engineering and Processing: Process Intensification*, *46* (2007), 8, pp. 703-712
[23] Su, B., *et al.*, Large eddy simulation of flow and mixing characteristics in a T-junction under inflow pulsation, *Applied Thermal Engineering*, *181* (2020), p. 115924
[24] Lu, P., *et al.*, Analysis of pressure drop in T-junction and its effect on thermodynamic cycle efficiency, *Applied Energy*, *231* (2018), pp. 468-480
[25] Patiño-Jaramillo, G.A., *et al.*, Laminar flow and pressure loss in planar Tee joints: Pressure loss coefficients, *European Journal of Mechanics - B/Fluids*, *94* (2022), pp. 263-275
[26] Lei, X.-s., *et al.*, Parametric study and optimization of dimpled tubes based on Response Surface Methodology and desirability approach, *International Journal of Heat and Mass Transfer*, *142* (2019), p. 118453
[27] Tang, Y., *et al.*, Multi-objective optimization of methanol reforming reactor performance based on response surface methodology and multi-objective particle swarm optimization coupling algorithm for on-line hydrogen production, *Energy Conversion and Management*, *307* (2024), p. 118377
[28] Qader, B.S., *et al.*, RSM approach for modeling and optimization of designing parameters for inclined fins of solar air heater, *Renewable Energy*, *136* (2019), pp. 48-68
[29] Manmai, N., *et al.*, Bioethanol production from sunflower stalk: application of chemical and biological pretreatments by response surface methodology (RSM), *Biomass Conversion and Biorefinery*, *11* (2021), 5, pp. 1759-1773

Submitted: 29.07.2025.
Revised: 24.09.2025.
Accepted: 26.09.2025.